Effect of E1(64–81) hepatitis G peptide on the *in vitro* interaction of HIV-1 fusion peptide with membrane models

Maria Jesús Sánchez-Martín [a],*, M. Antònia Busquets [a], Victoria Girona [a], Isabel Haro [b], M. Asunción Alsina [a], Montserrat Pujol [a]

[a] Physical Chemistry Department, Faculty of Pharmacy, University of Barcelona, CSIC-Associated Unit: Peptides and Proteins: Physicochemical Studies, IN2UB Av. Joan XXIII s/n, 08028 Barcelona, Spain
[b] Unit of Synthesis and Biomedical Application of Peptides, Department of Biomedical Chemistry, IQAC-CSIC, Jordi Girona 18, 08034, Barcelona, Spain

ARTICLE INFO

ABSTRACT

One way to gain information about the fusogenic potential of virus-derived synthetic peptides is to examine their interfacial properties and subsequently to study them in monolayers and bilayers. Here, we characterize the physicochemical surface properties of the peptide E1(64–81), whose sequence is AQLVGELGSLYGPLSVSA. This peptide is derived from the E1 structural protein of GBV-C/HGV which was previously shown to inhibit leakage of vesicular contents caused by the HIV-1 fusion peptide (HIV-1 FP). Mixed isotherms of E1(64–81) and HIV-1 FP were obtained and their Brewster angle microscopy (BAM) and atomic force microscopy (AFM) images showed that the peptide mixture forms a different structure that is not present in the pure peptide images. Studies with lipid monolayers (1,2-dimyristoyl-*sn*-glycero-3-[phospho-*rac*-(1-glycerol)] (DMPG) and 1,2-dipalmitoyl-*sn*-glycero-3-phospho-*rac*-(1-glycerol) (DPPG)) show that both peptides interact with all the lipids assayed but the effect that HIV-1 FP has on the monolayers is reduced in the presence of E1(64–81). Moreover, differential scanning calorimetry (DSC) experiments show the capacity of HIV-1 FP to modify the properties of the bilayer structure and the capacity of E1(64–81) to inhibit these modifications. Our results indicate that E1(64–81) interacts with HIV-1 FP to form a new structure, and that this may be the cause of the previously observed inhibition of the activity of HIV-1 FP by E1(64–81).

© 2011 Elsevier B.V. All rights reserved.

1. Introduction

The independently discovered human viruses GB virus C (GBV-C) [1] and hepatitis G virus (HGV) [2] are two isolates of the same single-stranded RNA virus. GBV-C/HGV shows characteristics of a *flavivirus*-like genome, closely related to the hepatitis C virus (HCV).

GBV-C/HGV is widely spread as a result of blood transfusions and sexual transmission. The virus infects lymphocytes, but not hepatocytes and there is no conclusive evidence of a causal link between GBV-C/HGV and either acute or chronic liver disease. Recently, GBV-C/HGV has been studied in the context of human immunodeficiency virus (HIV) infection and there are reports that co-infection prolonged survival of patients and therefore is potentially an effective treatment [3–5].

Based on a co-infection model, GBV-C/HGV may influence HIV disease via inhibition of HIV by inducing chemokines, down-regulating the HIV co-receptor(s), influencing cytokine profiles, or having other—as yet undefined—effects on the host lymphocytes [4,5]. However, the mechanism responsible for the beneficial effect that the GBV-C/HGV virus has on the course of disease caused by HIV infection has not yet been identified.

The envelope proteins (E) of flaviviruses have been described as class II fusion proteins [6], characterized by putative fusion sequences known as fusion peptides. The capacity of these fragments for vesicle fusion and cell lysis seems to correlate with the strong interaction these peptides have with membranes.

Bearing in mind the potential use of synthetic peptides as antiviral therapies, our group is currently examining the capacity of GBV-C/HGV synthetic peptides to interact with and induce fusion in model membranes [7,8]. The capacity, observed *in vitro*, to inhibit the leakage of vesicular contents caused by the HIV-1 fusion peptide (HIV-1 FP) [9] is the property that allows us to select the sequences of the envelop protein E1 of GBV-C/HGV in order to study their interaction with model membranes and with HIV-1 FP.

In this work, an epitope of GBV-C/HGV located in the (64–81) region of the E1 structural protein is selected as a possible inhibitor of the activity of HIV-1 FP. This epitope has also been demonstrated not to be cytotoxic *in vivo* and is therefore an interesting sequence to study. The aim of this work is to study the effect of the E1(64–81) peptide on the activity of the peptide sequence that represents the 23 N-terminal residues of the surface protein gp41 of HIV which corresponds to HIV-1 FP. Both peptide sequences are physicochemically characterized by

* Corresponding author. Tel.: +34 93 402 45 58; fax: +34 93 403 59 87.
E-mail address: mjsanchez@ub.edu (M.J. Sánchez-Martín).

studying their interaction with model membranes; lipopeptide interactions with lipid monolayers of 1,2-dimyiristoyl-*sn*-glycero-3-[phospho-*rac*-(1-glycerol)] (DMPG) and 1,2-dipalmitoyl-*sn*-glycero-3-phospho-*rac*-(1-glycerol) (DPPG) are studied. In addition, Langmuir monolayers are examined by Brewster angle microscopy (BAM) and atomic force microscopy (AFM). We also study the capacity of the E1 (64–81) peptide sequence to inhibit the interaction with and destabilization of membranes induced by the HIV-1 FP glycoprotein. Moreover, peptide–peptide interactions are characterized by means of Langmuir monolayers and the thermotropic behavior of DMPG and DPPG multilamellar vesicles (MLV) is studied by differential scanning calorimetry (DSC), in the absence and in the presence of E1(64–81) and HIV-1 FP, in view of the fact that lipid membranes are characterized by one main phase transition between an ordered gel state and a disordered liquid-crystalline phase, and that they could be affected by the interaction of the peptides with the bilayer.

2. Experimental

2.1. Materials

Amino acids and Rink amide resin (Tentagel R RAM, 0.19 meq g^{-1}) were obtained from *Novabiochem* (Nottingham, UK). Dimethylformamide (DMF) was purchased from *Scharlau* (Barcelona, Spain). Dichloromethane (DCM) and piperidine were purchased from *Fluka* (Neu-Ulm, Germany). The washing solvents acetic acid, diethyl ether, and trifluoroacetic acid (TFA) were obtained from *Merck* (Poole, UK). *N*-hydroxybenzotriazole (HOBt) and *N,N'*-diisopropylcarbodiimide (DIPCDI) coupling reagents were obtained from *Fluka* and *Novabiochem*, respectively. The other coupling reagents, O-(7-Azabenzotriazole-1-yl)-*N*, *N,N'N'*-tetramethyluronium hexafluorophosphate (HATU) and *N,N'*-diisopropylethylenamine (DEIA), were obtained from *GenScript Corporation* and *Fluka*, respectively. The scavengers ethanedithiol (EDT) and triisopropylsilane (TIS) were from Sigma-Aldrich.

1,2-dimyristoyl-*sn*-glycero-3-[phospho-*rac*-(1-glycerol)] (DMPG) and 1,2-dipalmitoyl-*sn*-glycero-3-phospho-*rac*-(1-glycerol) (DPPG) were purchased from Avanti Polar Lipids. Their purity was more than 99% and they were used without further purification.

Chloroform and methanol were purchased from Merck. Water was double distilled and deionized (MilliQ system, Millipore) (18.2 MΩ cm, pH 5.8). The buffer in all experiments was HEPES (from Sigma-Aldrich) 5 mM and NaCl (from Merck) 20 mM, pH 7.4.

2.2. Methods

2.2.1. Peptide synthesis

Synthesis of the peptide E1(64–81), whose primary amino acid sequence is: AQLVGELGSLYGPLSVSA, was carried out on a Tentagel R RAM resin (0.19 meq g^{-1}), by a solid phase methodology following an Fmoc/tBu strategy by means of DIPCD/HOBt activation [10]. For difficult couplings, HATU and DEIA agents were used. Side protection was effected by: 2,2,5,7,8-pentamethyl-chroman-6-sulfonyl (Pmc) for Arg; tert-Butyl (tBu) for Tyr, Ser, Thr and Asp; and t-butyloxycarbonyl (Boc) for Lys and Trp.

A threefold molar excess of Fmoc-amino acids was used throughout the synthesis. The stepwise addition of each residue was assessed by Kaiser's (ninhydrin) test [11] and couplings were repeated when the test result was positive.

The synthesized peptide was deprotected from the side-chain groups and cleaved from the resin with a treatment of trifluoroacetic acid (TFA) containing appropriate proportions of the scavengers [12] H$_2$O, triisopropylsilane (TIS), and ethanedithiol (EDT): 94.0% TFA; 2.5% H$_2$O; 2.5% EDT; 1% TIS.

The peptide was characterized by Perkin Elmer analytical HPLC with an LC-235 Diode Array Detector and a Binary LC Pump 250; the column used was a 25 × 0.46-cm KROMASIL 100 C18 5 μm. The analysis was carried out using a linear gradient of 95% H$_2$O (0.05% TFA)/5% acetonitrile (0.05% TFA) to 5% H$_2$O (0.05% TFA)/95% acetonitrile (0.05% TFA). Characterization by electrospray mass spectrometry was carried out by UPLC-MS (Waters ACQUITY Ultra Performance LC™, using a 2.1 × 100-mm BEH C18 1.7 μm column).

HIV-1 FP/AVGIGALFLGFLGAAGSTMGAAS was synthesized in the same way but using a ChemMatrix 100% polyethyleneglycol-based resin.

2.2.2. Surface activity of E1(64–81)

Experimental measurements were recorded with a NIMA Langmuir Film Balance equipped with a Wilhelmy platinum plate (NIMA Technology, Coventry, UK) and a Teflon trough that was rinsed with ethanol and distilled water before use. All experiments were performed at room temperature.

The surface activity of the peptide was first studied to determine the equilibrium spreading pressure. Using a cylindrical PTFE trough (19.6 cm^2, 27.2 cm^3), increasing volumes of 0.28 mM peptide solution in acetonitrile/H$_2$O (1:1, v/v) were injected below the HEPES subphase (pH 7.4) through a lateral hole and the adsorption of the peptide at the air/water interface was monitored by observing the increase in surface pressure as a function of time under continuous stirring of the subphase.

2.2.3. Insertion of peptide into monolayers

The kinetics of insertion of E1(64–81) into monolayers of DMPG and DPPG were measured using the same trough as for the surface activity, which was cleaned in the same way with ethanol and distilled water before use. For these experiments, a lipid stock solution in chloroform/methanol (2:1, v/v) was prepared and added dropwise onto the subphase until the desired lipid pressure was achieved. After 10–20 min, the lipid monolayer reached equilibrium. Then, 0.28 mM E1(64–81) solution in acetonitrile/H$_2$O (1:1, v/v) was injected into the subphase through the side hole of the trough. The subphase was magnetically stirred during the measurements and surface pressure changes were monitored as a function of time until the pressure remained constant.

2.2.4. Compression isotherms

Compression isotherms were established in a NIMA Langmuir Teflon trough (surface area 595 cm^2, volume 297.5 cm^3) with two moving Teflon barriers, which was also rinsed with ethanol and distilled water before use. By depositing appropriate volumes of chloroform/methanol (2:1, v/v) stock solutions of phospholipids (0.28 mM) and of peptides (0.28 mM), lipid–peptide spreading solutions were obtained. Monolayers were formed by applying small drops of the spreading solutions onto the HEPES subphase (pH 7.4) with a micro syringe (Hamilton Co., Reno, NV, USA). After 15 min, monolayers of the desired composition were continuously compressed with a rate of area reduction of 15 cm^2 min^{-1}; the area reduction rate ranges from 4.45 to 8.89 Å^2 molecule^{-1} min^{-1} depending on the volume injected for each sample necessary to achieve the collapse. The films were compressed to their collapse pressure when possible. Each run was repeated three times and the reproducibility was ±1 ^{2} molecule^{-1}.

2.2.5. Brewster angle microscopy

BAM images were obtained on a MicroBAM3 instrument (NIMA Technology) mounted on a NIMA Langmuir balance trough. The instrument was equipped with a 30-mW laser emitting p-polarized light at 659 nm, which incises the air–water interface at 53.1° (Brewster angle). All the images were taken at room temperature.

2.2.6. DSC experiments

Multilamellar lipid vesicles of DMPG and DPPG were prepared for DSC measurements in a VP-DSC Microcalorimeter (MicroCal LLC,

Northampton, MA, USA). The lipids and the peptides were dissolved in a chloroform/methanol mixture (2:1, v/v). Mixtures of different lipid and peptide compositions were prepared and they were evaporated to dryness in vacuum. Then, the films were hydrated with HEPES buffer (5 mM, pH 7.4) to obtain MLVs [13].

2.2.7. AFM imaging

AFM experiments were performed with a multimode microscope controlled by Nanoscope IIIa electronics (Digital Instruments, Santa Barbara, CA, USA). Images were acquired in tapping mode (TM-AFM) at minimum vertical force, maximizing the amplitude set point value and maintaining the vibration amplitude as low as possible.

A KSV5000 Langmuir film balance with a Wilhelmy platinum plate and a Teflon® trough with a surface of 185 cm^2 (maximum opened barriers) and two moving Teflon® barriers were used. Deposition of monolayers was onto a fresh mica substrate (Green Muscovite Mica disks: Metafix, Montdidier, France) at constant surface pressure for the AFM study. During the film transfer to mica, the surface pressure was kept constant by the use of a feedback system. Before taking the measurements, the mica disks were glued onto a steel disk using a water-insoluble epoxy, and they were then set on the piezoelectric scanner.

2.2.8. Circular dichroism

Circular dichroism (CD) spectra were recorded on a Jasco J-810 spectropolarimeter (Japan Spectroscopic Company, Tokyo, Japan). All measurements were taken in water and trifluoroethanol (TFE). Cells 1 cm in diameter were used and the spectra were measured between 190 and 260 nm using a spectral bandwidth of 1 nm and a scan speed of 10 nm/min.

All measurements were performed at 25 °C and the data were expressed in terms of mean residue ellipticities [θ] (deg cm^2 dmol^{-1}). Three scans were performed to improve the signal to noise ratio. E1 (64–81) was incubated with POPG liposomes before the peptide spectrum was observed. Finally, a spectrum of the blank solution (POPG liposomes) was subtracted from the peptide spectrum and the data converted to mean residue ellipticity units [14]. The Contin program from the Dichroweb server at http://dichroweb.cryst.bbk.ac. uk/html/home.shtml was used to treat experimental CD results [15,16].

3. Results and discussion

3.1. Peptide–peptide interaction

3.1.1. Adsorption kinetic of E1(64–81)

A small gradual adsorption of E1(64–81) was observed at low peptide concentrations. The higher the peptide concentration in the subphase, the faster the incorporation process and the higher the surface pressure attained. Experiments were carried out for more than an hour in all cases but after 30 min the pressure remained constant and we considered that at this time equilibrium had been reached. Fig. 1 shows the adsorption isotherm profile for E1(64–81). The shape of the surface activity curve approximates a rectangular hyperbola and it was fitted to Eq. (1) via non-linear least squares regression analysis.

$$\pi = \frac{C\,\pi_{max}}{K + C} \tag{1}$$

Where C is the concentration, π_{max} is the maximum pressure achieved and K is a characteristic constant equal to the peptide concentration that yields $\frac{1}{2}\pi_{max}$. Fitting the data, the values obtained for E1(64–81) were 17.05 mN m^{-1} for π_{max} and 0.20 μM for K ($R^2 = 0.982$). Peptide concentrations corresponding to this K value were chosen for further penetration studies, as it corresponds to the
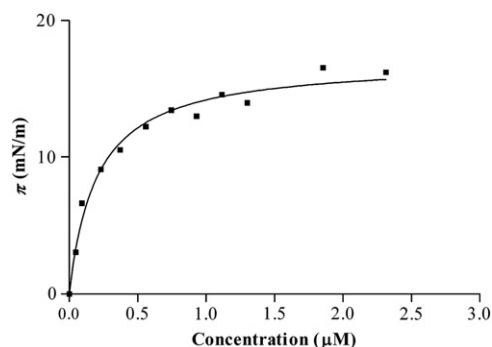

Fig. 1. Surface activity curve of E1(64–81).

concentration of the peptide that should be used in the bulk subphase for penetration kinetics experiments, lower than the equilibrium spreading pressure of the peptide [17].

By applying the Gibbs adsorption equation in its simple form (Eq. (2)) it is possible to calculate the peptide surface excess concentration (Γ):

$$\Gamma = \frac{\Delta\pi}{RT\Delta\,\ln C} \tag{2}$$

where R is the gas constant (8.31 J K^{-1} mol^{-1}), T is the temperature (298 K), $\Delta\pi$ is the pressure increase achieved 30 min after injection and C is the peptide concentration.

The surface excess concentration of E1(64–81) at saturation (Γ_{max}) deduced from the slope of the $\Delta\pi - \ln C$ curve (Eq. (2)) was 1.34×10^{-6} mol m^{-2}. This value allows us to calculate the surface molecular area by means of Eq. (3), where N is Avogadro's constant.

$$A = \frac{1}{\Gamma_{max}}N. \tag{3}$$

The molecular area obtained was 1.24 nm^2 molecule^{-1}. This value is compatible with an α-helical conformation of the peptide and with vertical orientation at the air–water interface [8,18,19], which was corroborated by means of CD experiments (Section 3.1.2).

3.1.2. Circular dichroism of E1(64–81)

CD experiments and the corresponding quantitative analysis of the experimental data using a deconvolution computer program were performed. In general, short synthetic peptides do not have a preferential conformation in solution, but they can sometimes adopt moderately stable secondary structures [20]. The CD experiments were carried out in the presence of POPG liposomes and the resulting spectrum is shown in Fig. 2. The negative bands located at 205 and 222 nm and the positive band around 195 nm are characteristic of an α-helix structure.

3.1.3. Miscibility studies of E1(64–81) and HIV-1 FP

To study the miscibility of the peptides E1(64–81) and HIV-1 FP, the compression isotherms of each of them and those of their mixtures were recorded (Fig. 3).

Firstly, studying the E1(64–81) isotherm, we can observe that at 17 mN m^{-1}, when lateral compression takes place [21], the molecular area was 1.25 nm^2 molecule^{-1} (Fig. 3). This value, obtained from a dynamic system, is the same as that obtained from Eq. (3). The value is of the same order as those obtained by other authors for peptides of similar amino acid chain length and similar hydrophobic profiles based on their primary sequence; Ambroggio et al. [18] found a molecular area of 1.80 nm^2 molecule^{-1} for citropin, a 16-amino-acid antibiotic peptide. Moreover, it is similar to the molecular area of an α-helix perpendicular
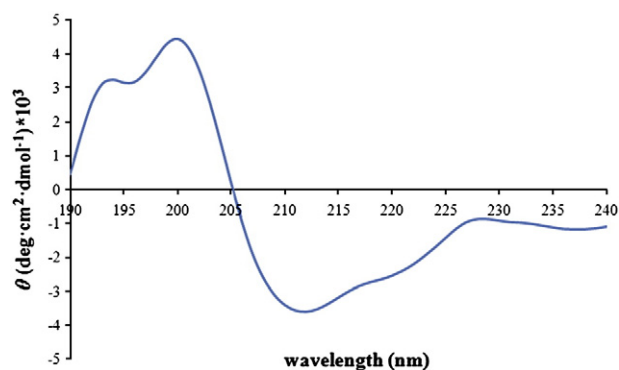
Fig. 2. CD spectra of E1(64–81) in the presence of POPG liposomes.

to the interface, as reported by Conn et al., which was 1.30 nm²[22]. Furthermore, the limiting area (A_o) calculated by extrapolation of the steep part of the isotherm with the area axis [21], agrees with the published theoretical values and a plateau can be seen where the collapse of the monolayer takes place. Ambroggio et al.[18] obtained 1.75 nm² as the theoretical A_o value for an α-helix peptide oriented perpendicular to the interface; 1.80 nm² has been published for an ideal HIV-1 FP α-helix secondary structure, as calculated by molecular modeling [23]. In our case, the extrapolated value (1.75 nm² molecule^{-1}) is greater than the value of 1.25 nm² found at 17 mN m^{-1}, very close to the pressure that we postulated as the monolayer collapse (17.6 mN m^{-1}) based on BAM images recorded at this point. However, collapse does not disrupt the monolayer but the compressibility does change at the plateau (see below). This fact allows higher values of pressure to be achieved in the steep part of the isotherm where the partial immersion of polar groups of the peptide or folding of the hydrophobic part are also possible.

From π-A, at low surface pressures (0–10 mN m^{-1}), it can be observed that the addition of HIV-1 FP to the E1(64–81) monolayer produces higher values of the mean molecular area as the proportion increases, indicating interactions between the two peptides. Large positive deviations observed at E1(64–81) mole fraction values in the range $0.4 \geq X_{E1(64-81)} \geq 0.2$, suggest that the E1(64–81)/HIV-1 FP complex forms clusters in the monolayer.

As can be seen, at a surface pressure of 17 mN m^{-1}, the isotherms of both peptides present a transition represented by a plateau. This has been explained in different ways. It is possible that it was the result of the formation of a bilayer [24] or of the molecular segments
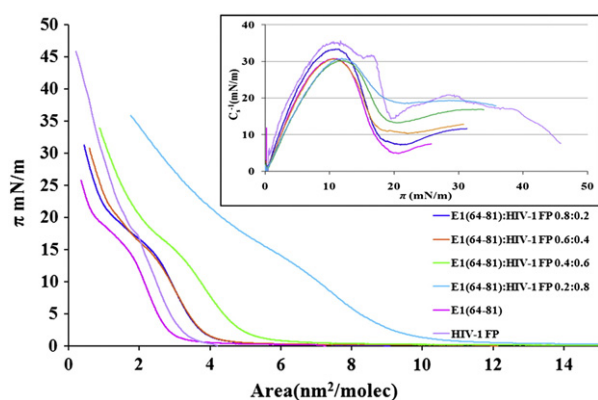
being lifted from the water surface [25], or of a change in orientation of the molecules upon compression [26], or it could correspond to a rearrangement of the molecules as described in the literature for other peptides with similar characteristics (area per molecule, A_o, and the absence of clear collapse pressure in compression isotherm register) [27,28]. The inset in Fig. 3 shows the values of the surface compressibility modulus (C_s^{-1}) corresponding to each isotherm. These values were calculated by applying Eq. (4).

$$C_s^{-1} = -A \left[\frac{\partial \pi}{\partial A} \right]_T. \tag{4}$$

Where A is the area per molecule at the indicated surface pressure and π is the corresponding surface pressure.

The surface compressibility modulus can be used to characterize the phase state of the monolayer [29] (for liquid expanded films it ranges from 12.5 to 50 mN m^{-1}, while for the liquid condensed phase it ranges from 100 to 250 mN m^{-1}) [30].

In our case, the values of C_s^{-1} indicate that the monolayers are in the liquid expanded state before and after the transition plateau. The extension of this plateau decreases as the HIV-1 FP mole fraction increases, as can be seen in the inset in Fig. 3.
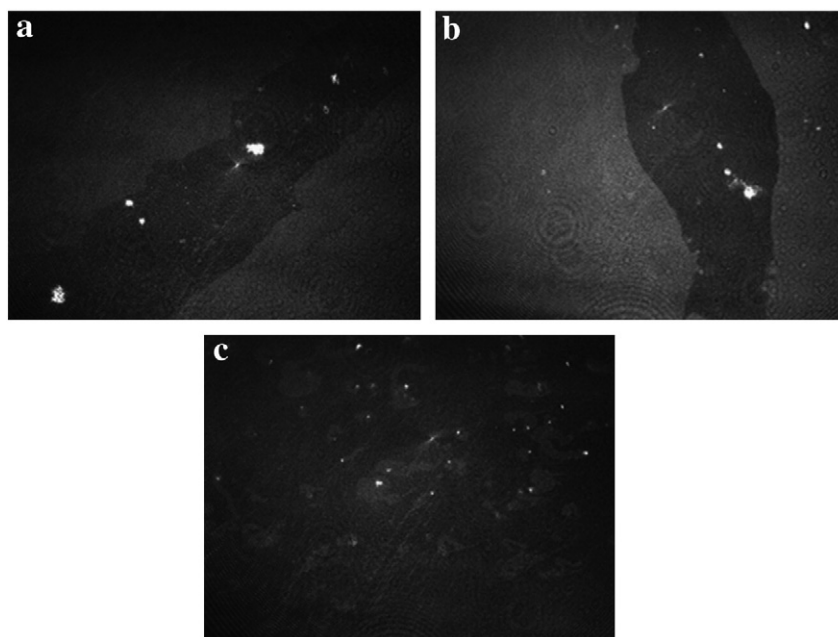
To study what happens, the phase behavior of the E1(64–81)/HIV-1 FP system was morphologically examined using BAM and AFM. Figs. 4 and 5 show the BAM and AFM images respectively, corresponding to both peptides separately and to the mixture, where $X_{E1(64-81)} = 0.6$, at a pressure of 10 mN m^{-1} when the monolayers are in the liquid expanded state.

As can be seen in the BAM images, each peptide individually presents the coexistence of two phases: gas and liquid. However, in the mixture, we observe a new liquid phase, indicating an interaction between the peptides. This interaction can also be observed in the AFM images where the pure peptide LB films are quite different from the LB film of the mixture, corroborating that the structure of the peptides separately is different from that of the mixture at the same pressure. Firstly, E1(64–81) and HIV-1 FP (Fig. 5a and b) both present round particles that are ordered differently depending on the peptide.

The E1(64–81) LB film (Fig. 5a and d) shows a non-uniform extension of the peptide on the mica surface. The LB film presents large uncovered regions while the monolayer surface had a granular roughness with small round holes. The monolayer thickness was determined as the step height from the uncovered mica surface (the darkest regions in Fig. 5a and d) and the layer, to give a main height of 1.8 ± 0.2 nm. Meanwhile, for HIV-1 FP, and its mixture with E1(64–81), (Fig. 5b/e and c/f, respectively), the peptide monolayers are more uniform and the mica surface cannot be observed. Furthermore, in the LB mixed film, we can observe curly filaments of a similar shape and size covering the surface that were not present in the LB films of the pure peptides. This suggests similar peptide behavior to that observed in the BAM images.

To gain insight into the interactions established between E1(64–81) and HIV-1 FP, a thermodynamic point of view was considered and the excess Gibbs energy of mixing (ΔG_M^{EX}) was calculated. The ΔG_M^{EX} values provide us with further information on the energy of the mixing process and the specific interactions of the two components. Positive values indicate that the process of mixing is not thermodynamically favorable, so the mutual interactions between the two components are weaker than the interactions between the pure component molecules themselves. Negative values indicate that the process is thermodynamically favorable. It must also be noted that when $|\Delta G_M^{EX}| < RT$, the differences from ideality are not considered statistically significant and the mixture can be considered ideal [31].

ΔG_M^{EX} was calculated using Eq. (5)[32] where N_A is Avogadro's number, A_{12} is the mean area per molecule in the mixed film, A_1 and

**Fig. 3.** Surface pressure–mean area per molecule (π-A) compression isotherms of E1(64–81), HIV-1 FP and their mixtures spread on a HEPES subphase. Inset: plot of compressibility modulus (C_s^{-1}) as a function of the surface pressure.

Fig. 4. 4.1×3.6 mm^2 BAM images corresponding to the monolayers of: a) E1(64–81); b)HIV-1 FP; and c) E1(64–81):HIV-1 FP at a molar ratio of 0.6:0.4, spread on HEPES at a surface pressure of 10 mN m^{-1}.

A_2 are the areas per molecule in the pure films, X_1 and X_2 are the molar fractions, and π is the surface pressure (mN m^{-1}).

$$\Delta G_M^{EX} = N_A \int_{\pi \to 0}^{\pi} A_{12} d\pi - X_1 \int_{\pi \to 0}^{\pi} A_1 d\pi - X_2 \int_{\pi \to 0}^{\pi} A_2 d\pi. \tag{5}$$

Table 1 shows the ΔG_M^{EX} values calculated for the peptide–peptide mixtures assayed at different surface pressures. In all cases, it can be seen that $|\Delta G_M^{EX}|$ values increase with the HIV-1 FP mole fraction. At surface pressures of 10 mN m^{-1} or lower and $X_{E1(64–81)} \geq 0.6$, the mixtures have $|\Delta G_M^{EX}| < RT$ so they can be considered ideal and the
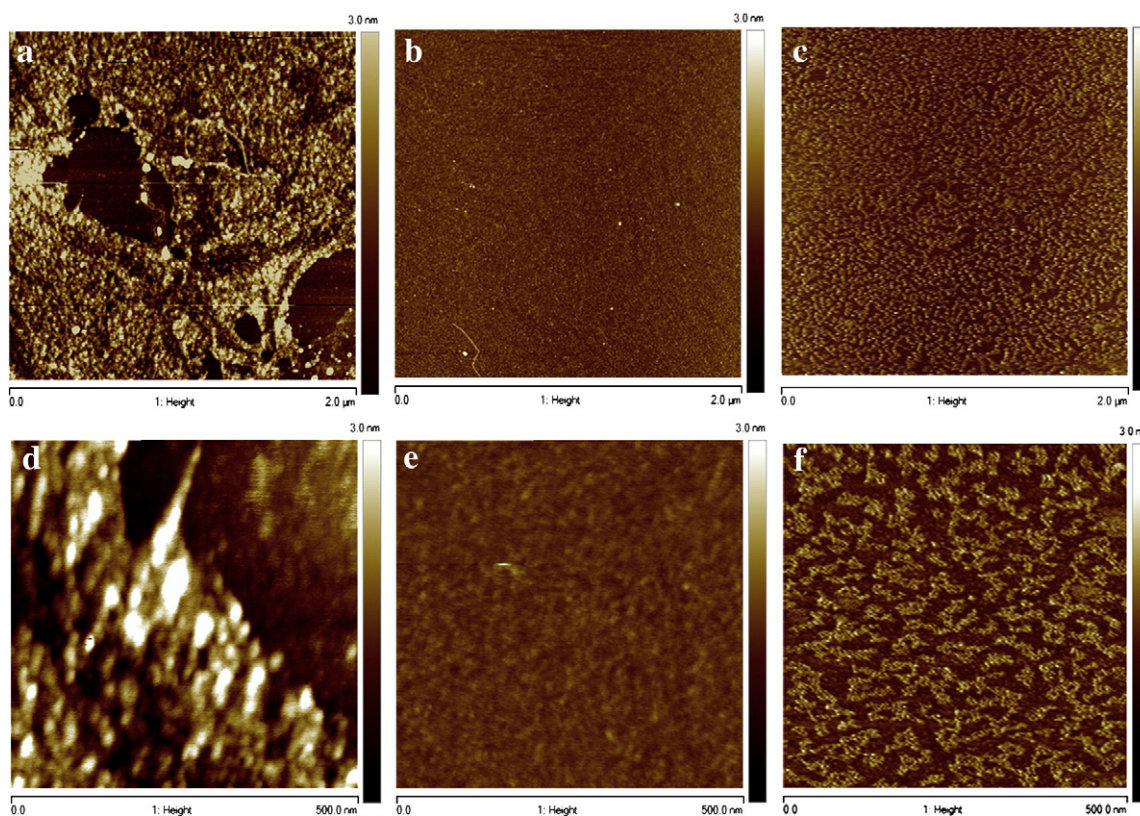
Fig. 5. LB films of 2×2 μm (top) and 500×500 nm (bottom) at an extraction surface pressure of 10 mN m^{-1}: a) and d) E1(64–81); b) and e) HIV-1 FP; and c) and f) E1(64–81):HIV-1 FP at a molar ratio of 0.6:0.4.

Table 1
G_M^{EX} (J mol^{-1}) for different HIV-1 FP-E1(64–81) mixtures at various pressures.

$X_{E1(64–81)}$	π (mN m^{-1})	ΔG^{ex} (J mol^{-1})
0.2	5	4494
	10	8073
	20	23766
	25	31990
0.4	5	2146
	10	3352
	20	8727
	25	10980
0.6	5	814
	10	1360
	20	3861
	25	5515
0.8	5	294
	10	701
	20	3894
	25	5909

interactions between the two components and between each component itself are the same. In contrast, for pressures higher than 10 mN m^{-1} and when the concentration of HIV-1 FP is higher than the E1(64–81) concentration, $|\Delta G_M^{EX}|$ values are greater than RT and positive in all cases.

3.2. Peptide–lipid interactions

The characterization of membrane interactions with peptides or proteins is important for a better understanding of their mode of action. In order to determine some peptide–lipid binding properties, a monolayer approach is used where the peptides are inserted into the lipid monolayer.

3.2.1. Penetration kinetics

The capacity of the peptide E1(64–81) to penetrate into phospholipid monolayers was studied using a 0.200 μM peptide solution in the HEPES-buffered subphase, which corresponds to the K calculated from Eq. (1). Fig. 6 shows surface pressure increases ($\Delta\pi$) due to the introduction of E1(64–81) in monolayers of different phospholipids, over the initial lipid pressure (π_i). For both lipids, the general trend observed is that the greater the π_i, the lower the degree of incorporation of the peptide into the monolayer because of the closer packing of the lipids at higher initial pressures.

The monolayer exclusion pressure (that is, the surface pressure above which the peptide does not penetrate into the monolayer) was obtained by extrapolating the plot to $\Delta\pi = 0$ mN m^{-1} (Fig. 6) [33]. It can be seen that the peptide interacts with the two lipids tested; however, a stronger interaction was observed when the monolayer was composed of DMPG. In this case, the exclusion pressure was
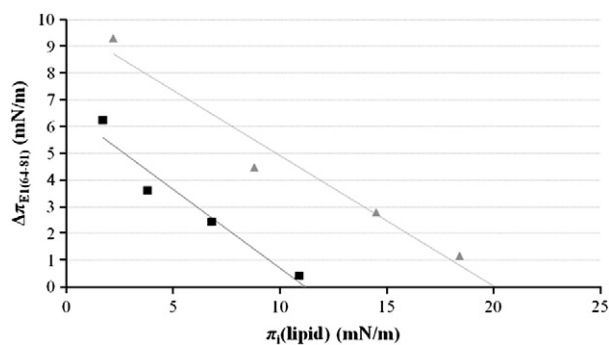
20.06 mN m^{-1}, clearly higher than that obtained when the monolayer was of DPPG (11.18 mN m^{-1}). DPPG and DMPG differ in their hydrocarbonated chains. For DPPG, which presents a higher C_s^{-1} value, the exclusion pressure is lower than that obtained for DMPG in a liquid expanded state, which with its lower C_s^{-1} value is a less rigid monolayer and, therefore, easier to penetrate than a liquid condensed monolayer (see at Section 2.2.2 the miscibility study). This corroborates observations in other studies [28].

3.2.2. Lipid–peptide miscibility

To determine the effect of the peptide E1(64–81) on the state of phospholipid monolayers and better understand the lipid–peptide interaction that takes place, mixed monolayers of E1(64–81) and the two phospholipids were obtained and the compressibility modulus for all these systems was calculated according to Eq. (4).

Fig. 7 shows the shape of the π-A isotherms obtained and, in the insets, the variation of the compressibility modulus compared to the surface pressure.

For both phospholipids, the presence of E1(64–81) results in higher mean molecular areas of the monolayer than for the pure phospholipid monolayer at all the molar fractions assayed. For the DPPG monolayer (Fig. 7a) the π-A isotherm shows a phase transition at a pressure of around 10 mN m^{-1} for pure DPPG, which is significantly modified when E1(64–81) is further incorporated into the monolayers. This phase transition shows as a minimum in the compressibility modulus. The same behavior can be observed for DMPG monolayers, where the phase transition of pure DMPG that occurs around 30 mN m^{-1} disappears when E1(64–81) is incorporated into the monolayer, and a minimum started to appear around 15 mN m^{-1}.

Fig. 6. Surface pressure increase ($\Delta\pi$) caused by E1(64–81) in monolayers of different phospholipids in front of the initial lipid pressure (π_i). Black squares correspond to DPPG and gray triangles to DMPG.
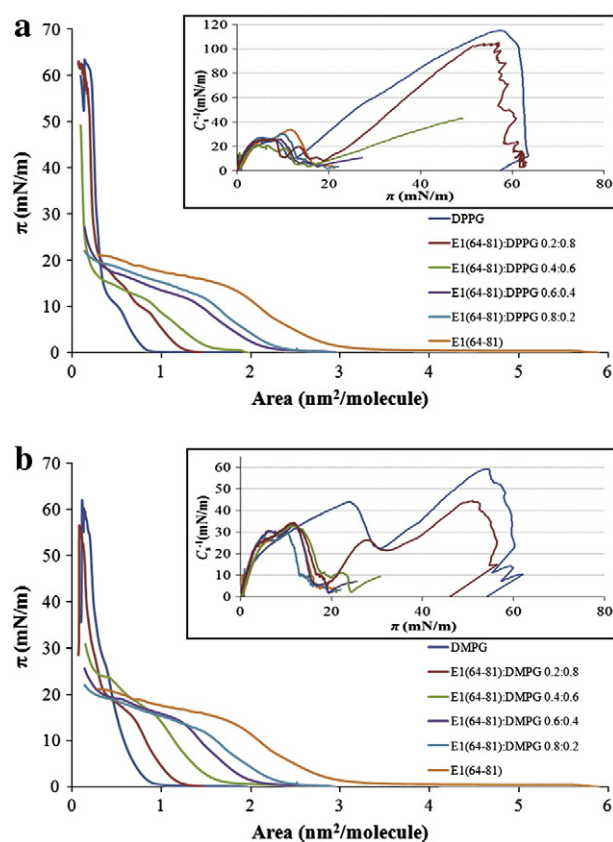

Fig. 7. Surface pressure–mean area per molecule (π-A) compression isotherms for E1(64–81) and the lipids: (a) DPPG and (b) DMPG spread on HEPES subphase (pH = 7.4) at different $X_{E1(64–81)}$. Insets: plots of compressibility modulus (C_s^{-1}) as a function of the surface pressure.

To further examine the miscibility of the film components, analysis of the collapse pressures can be helpful; the variation of π_c with the molar ratio of the components indicates two-dimensional miscibility. In our case, the collapse pressure of DPPG at 63 mN m^{-1} barely change when 20% E1(64–81) is added. However, for DMPG, adding the same percentage of peptide causes the collapse pressure to decrease to 55 mN m^{-1}. When the concentration of peptide is increased, for both phospholipids the collapse pressure decreases. The variation in the collapse pressure is indicative of miscibility: thus, in both cases we could see that the peptide and the phospholipids are miscible, but for DMPG, the earlier variation of the collapse pressure corroborates the results obtained in the exclusion pressure calculation where we observed that penetration into DMPG monolayers is easier than into DPPG monolayers.

To verify the effect of E1(64–81) on the state of phospholipid monolayers, the maximum compressibility modulus were calculated. Fig. 8 shows the values in function of peptide concentration. As indicated above, the incorporation of E1(64–81) into phospholipid monolayers causes a decrease in the C_{smax}^{-1} in all cases, hence, they are less condensed. This decrease is especially marked for DPPG monolayers of $X_{E1(64–81)} = 0.4$. Further additions of the peptide do not affect the value of C_{smax}^{-1}.

Evaluating the extent of intermolecular interactions in monolayers comprised of two components is aided by the application of the additivity rule. The additivity rule predicts that, in the case of an ideal mixture, the mean molecular area (A_{12}) at a given surface pressure will be equal to the weighted average:

$$A_{12} = X_1 A_1 + X_2 A_2 \qquad (7)$$

where A_1 and A_2 are the molecular areas of the single components at the same surface pressure and X_1 and X_2 are the mole fractions of components 1 and 2 in the mixed film. Comparison of the experimental mean molecular area with the expected values from the additivity rule, provides us with an important clue regarding the extent of miscibility and interactions in the binary monolayer. The linear dependence in the area–composition plots (Fig. 9) indicates ideal mixing or complete immiscibility of the components [34].

Analysis of the plots reveals small negative deviations from ideality at all $X_{E1(64–81)}$ molar fractions assayed and at different pressures (5, 10, 15 and 20 mN m^{-1}), suggesting that the peptide interacts with both phospholipids through attractive interactions [34,35].

The excess free energy of mixing for the E1(64–81) and DMPG or DPPG systems was calculated (Table 2).

A positive ΔG_M^{EX} reveals that peptide–lipid interactions are less favorable, while negative values show a more favorable interaction than between the pure components themselves. In general, the mixtures have $|\Delta G_M^{EX}| < RT$, so they can be considered ideal systems.
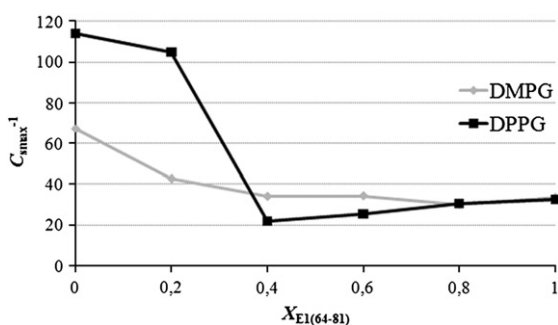
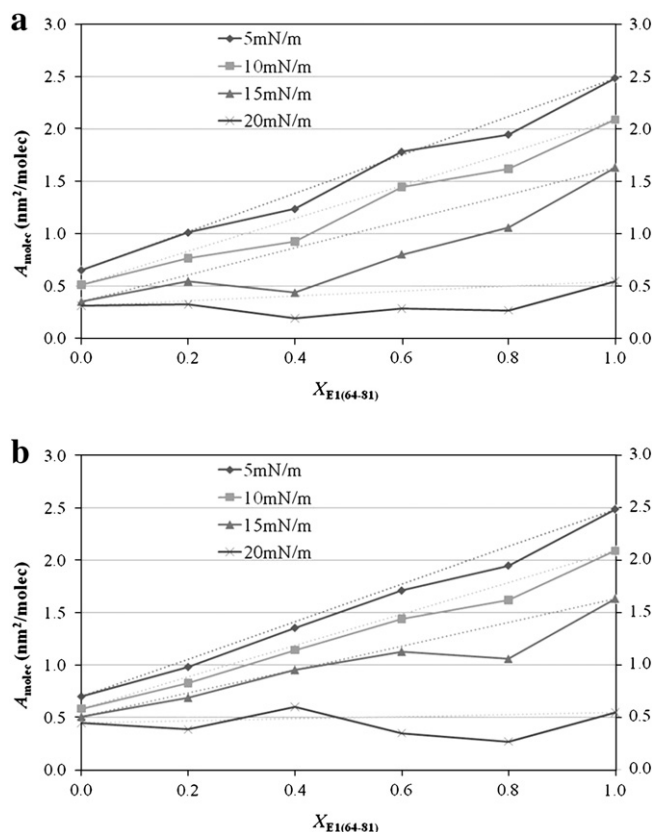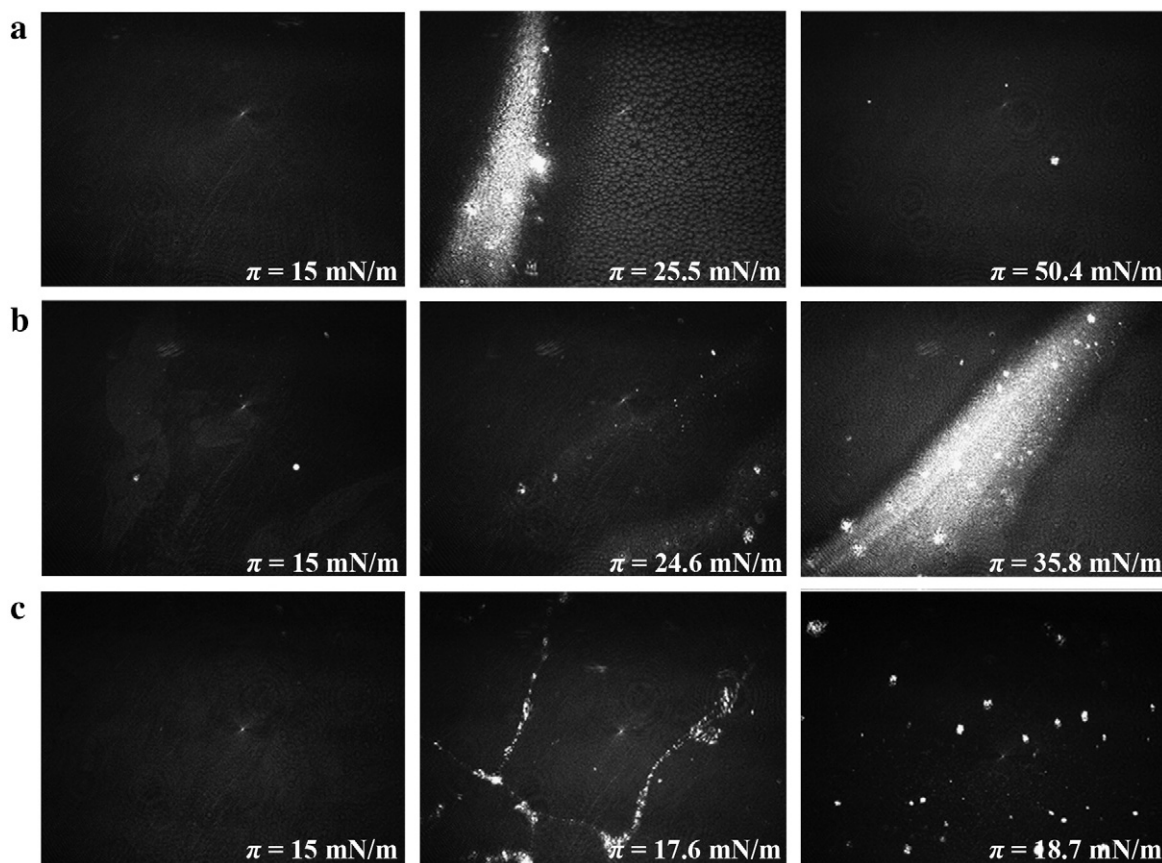**Fig. 8.** Maximum compressibility modulus values in function of peptide concentration for mixtures with DMPG and DPPG.

Fig. 9. Plots of A_{molec} for E1(64–81) as a function of the peptide molar fractions at different surface pressures for pure and mixed monolayers of: a) DPPG and b) DMPG. Dotted lines indicate ideality.

Fig. 10 shows miniBAM images of monolayers of pure DMPG (Fig. 10a), pure peptide (Fig. 10c) and a mixed monolayer of DMPG and the peptide at $X_{E1(64–81)} = 0.2$ (Fig. 10b). The pictures reveal that at pressures near 15 mN m^{-1}, the monolayer is homogeneous for pure DMPG and E1(64–81), whereas for the mixture, we can observe two different phases. This pressure corresponds to the beginning of the plateau where a change in the compressibility was observed; therefore we could say that two different phases co-exist in a liquid expanded state. At a pressure of 17.6 mN m^{-1}, peptide collapse could be observed (Fig. 10c); while this does not appear in the mixture

Table 2
G_M^{EX} (J mol^{-1}) for different lipid–E1(64–81) mixtures at various pressures.

$X_{E1(64–81)}$	ΔG^{ex} (J mol^{-1})		
	π (mN m^{-1})	DMPG	DPPG
0.2	5	−753	−737
	10	−780	−791
	15	618	486
	20	−238	−326
0.4	5	−504	−334
	10	−533	−111
	15	−470	2188
	20	721	590
0.6	5	−133	−257
	10	−196	55
	15	−523	1687
	20	−1694	−630
0.8	5	−317	−248
	10	−391	56
	15	−491	51
	20	−29	−235

Fig. 10. 4.1×3.6 mm^2 MiniBAM images of DMPG and E1(64–81) monolayers at three different pressures, and of their mixture: a) DMPG, b) DMPG:E1(64–81) at $X_{E1(64-81)} = 0.2$ and c) E1(64–81).

(not shown). This demonstrates the lipid–peptide miscibility. On the other hand, the phase transition observed for DMPG (Fig. 10a, at $\pi = 25.5$ mN m^{-1}) is clearly modified when DMPG is mixed with the peptide (Fig. 10b, at $\pi = 24.6$ mN m^{-1}). Moreover, the collapse observed for the mixture is very different from that of the pure components, showing a clear phase separation. In previous work, where the interaction of E1(145–162) hepatitis G virus peptide and DMPC, DMPG and POPG was studied, we reported similar behavior compatible with the formation of a peptide–lipid complex through hydrophobic interactions, which was corroborated when the interaction of the same peptide was studied in a bilayer system [8]. Hence, the higher mean molecular areas observed in monolayers due to E1(64–81) can be explained by the formation of the lipid–peptide complexes compatible with the BAM images and the phase separation observed when collapse is reached. This fact could be explained by the arrangement of a peptide–lipid complex and its separation from the lipid matrix.

3.2.3. E1(64–81)-HIV-1 FP–lipid miscibility

Fig. 11a shows the π-A compression isotherms for the HIV-1 FP and DPPG mixed system. HIV-1 FP addition shifts the isotherm to higher mean molecular areas at all the molar fractions assayed. Although the amino acid length is similar to that of E1(64–81), and both peptides present surface activity with π_{max} ranging from 17 to 20 mN m^{-1}, their miscibility pattern is quite different (Figs. 7a and 11a).

To examine the effect of E1(64–81) on the interaction of HIV-1 FP and phospholipids, mixed monolayers of both peptides and DPPG were studied. The proportion of E1(64–81):HIV-1 FP was 10:1 as in this proportion E1(64–81) was found to inhibit the percentage of leakage caused by HIV-1 FP [9]. Fig. 11b reveals the inhibition effect of E1(64–81) on the interaction of HIV-1 FP with a DPPG monolayer. The

shape of the π-A compression isotherms in Fig. 11b is very similar to that showed in Fig. 7a, corresponding to the E1(64–81)/DPPG mixed monolayers. Therefore, in the presence of E1(64–81) in vitro, HIV-1 FP cannot interact with DPPG.

The most significant difference can be seen by studying the compressibility modulus. We observe that the presence of HIV-1 FP makes the monolayer drastically change from a liquid condensed state to a liquid expanded state, while with E1(64–81) (Fig. 7a) or with the mixture of both peptides (Fig. 11b) we observe a transition between the phases when the peptide concentration is increased. Thus, the presence of E1(64–81) inhibits the capacity of HIV-1 FP to alter the compressibility of the monolayer.

This inhibition capacity was also studied with DSC experiments and can be attributed to the new species formed when both peptides are together, as can be seen in the BAM and AFM images (Figs. 4 and 5).

On the other hand, Fig. 12 shows the plots of the mean molecular area calculated from Eq. (7) against the composition. Analysis of Fig. 12a reveals small negative deviations from ideality at $X_{\text{HIV-1 FP}} = 0.2$ and at different pressures (5, 10, 15 and 20 mN m^{-1}), suggesting that the peptide interacts with the phospholipid through attractive interactions [34,35]. However, these deviations become positive at HIV-1 FP molar ratios higher than 0.2, although they are very small. The deviations become more positive for $X = 0.2$ and $X = 0.6$ when HIV-1 FP is mixed with E1(64–81), and more negative for $X_{E1(64-81) + \text{HIV-1 FP}} = 0.4$ showing a change in the behavior, but the deviations from ideality are too small to be considered significant.

The excess free energy of mixing for HIV-1 FP and HIV-1 FP + E1 (64–81) with DPPG was calculated (Table 3). All the mixtures have $|\Delta G_M^{EX}| < RT$, so they can be considered ideal systems.
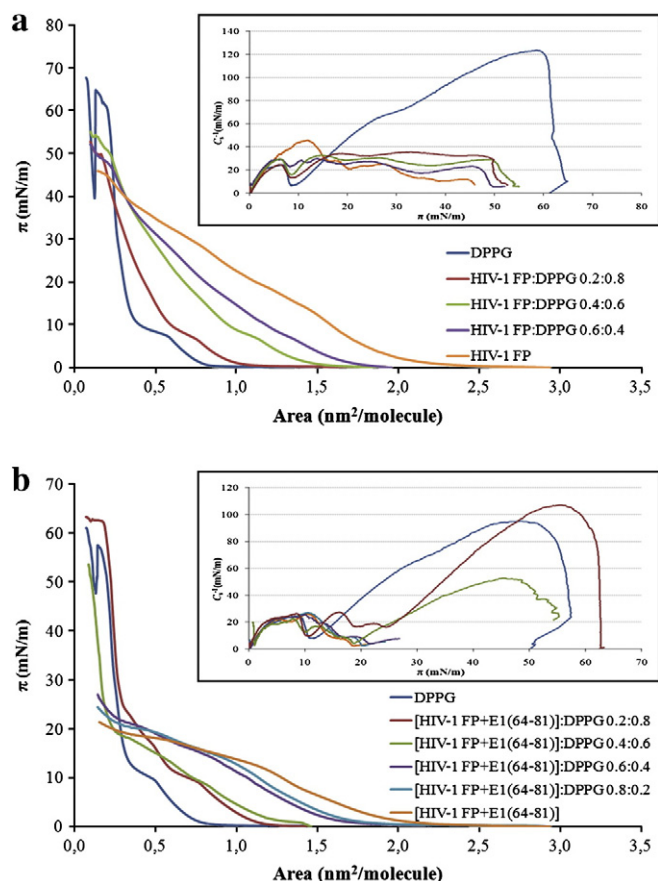
Fig. 11. Surface pressure–mean area per molecule (π-A) compression isotherms for: (a) HIV-1 FP and DPPG at different $X_{\text{HIV-1 FP}}$ and (b) E1(64–81), HIV-1 FP and DPPG at different $X_{\text{E1(64–81)-HIV-1 FP}}$, spread on HEPES subphase (pH = 7.4). Insets: plots of compressibility modulus (C_s^{-1}) as a function of the surface pressure.

3.2.4. DSC experiments

To study the modifications in the phase diagram produced by the insertion of the peptides into the bilayers, the binary DMPG/DPPG system was considered. The DMPG/DPPG phase diagram was constructed from DSC heating thermographs (scans were recorded between 10 °C and 60 °C) of the liposomes incubated with and without the peptide. In the heating thermographs (not shown) we could see how HIV-1 FP modifies the transition temperature (T_m) of the DPPG and DMPG liposomes, and how this temperature is again close to the T_m of pure phospholipids when HIV-1 FP is incubated with E1(64–81); this is clearly reflected in the phase diagrams.

The heat capacity curve of pure DMPG shows two phase transitions. The so-called pre-transition (T_p~20.7 °C for DMPG at pH = 7.4 in 5 mM HEPES + 20 mM NaCl) stands for a transition between two gel phases ($L_{\beta'} \rightarrow P_{\beta'}$). The main phase transition (T_m~23.8 °C) represents the transition from $P_{\beta'}$ gel to the liquid crystalline L_α phase. The phase diagram is constructed considering only the main phase transition [36].

The phase diagram is constructed by the following procedure: The onset and endset temperatures for the gel to liquid crystalline phase transition are determined as the temperatures corresponding to the intersection between the tangent of the leading edge and the baseline of the DSC curves [36–38]. For their contribution to the total transition widths, these temperatures need to be as follows [39]:

$$T_1 = T_{\text{onset}} + (X_A \Delta T_{1A} + X_B \Delta T_{1B}) \tag{8}$$

$$T_2 = T_{\text{endset}} - (X_A \Delta T_{2A} + X_B \Delta T_{2B}) \tag{9}$$
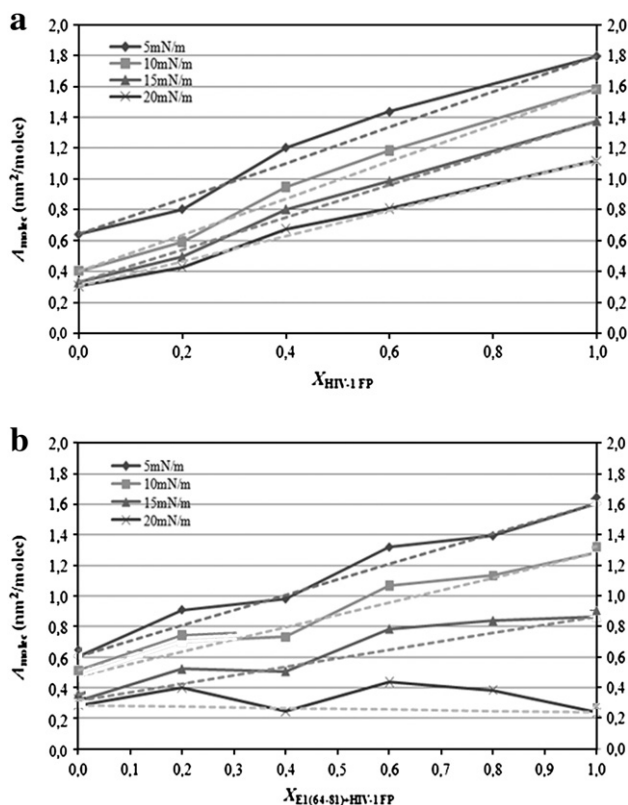
Fig. 12. Plots of A_{molec} as a function of the peptide molar fractions at different surface pressures for pure and mixed monolayers of: (a) HIV-1 and DPPG; and (b) HIV-1 FP + E1(64–81) and DPPG. Dotted lines indicate ideality.

where,

$$\Delta T_{1A} = T_m - T_{\text{onset}} \text{ for } X_{\text{DPPG}} = 1$$
$$\Delta T_{1B} = T_m - T_{\text{onset}} \text{ for } X_{\text{DPPG}} = 0$$
$$\Delta T_{2A} = T_{\text{endset}} - T_m \text{ for } X_{\text{DPPG}} = 1$$
$$\Delta T_{2B} = T_{\text{endset}} - T_m \text{ for } X_{\text{DPPG}} = 0.$$

X_A and X_B correspond to the molar fractions of lipids A (DPPG) and B (DMPG).
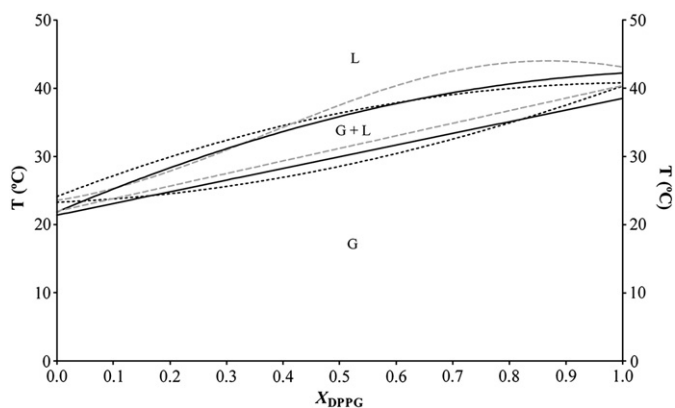
The temperatures calculated by Eqs. (8) and (9) are those represented in the phase diagram for each DPPG molar fraction (Fig. 13).

The shape of a phase diagram depends mainly on the mixing behavior of the lipids in both phases. For ideal miscibility of two lipids A and B, the *solidus* and *liquidus* curves enclose a cigar-shaped

Table 3
G_M^{EX} (J mol^{-1}) for different DPPG–HIV-1 FP mixtures and DPPG–HIV-1 FP + E1(64–81) mixtures at various pressures.

$X_{\text{PEPTIDE(S)}}$	ΔG^{ex} (J mol^{-1})		
	π (mN m^{-1})	HIV-1 FP:DPPG	HIV-1 FP + E1(64–81):DPPG
0.2	5	77	−65
	10	−42	121
	15	−71	−121
	20	−98	−418
0.4	5	11	−2
	10	122	196
	15	246	−54
	20	347	−150
0.6	5	−89	113
	10	28	134
	15	335	−107
	20	475	−601

Fig. 13. Phase diagram of DPPG:DMPG liposomes (solid lines) in the presence of HIV-1 FP (dashed gray lines) and in the presence of HIV-1 FP with E1(64–81) (dotted lines). G: Gel phase, L: Liquid crystalline phase.

coexistence region of the gel and liquid crystalline phases. Below the *solidus* curve, only the gel phase exists; and above the *liquidus* line, only a liquid crystalline phase appears [38]. The phase diagram confirms ideal mixing of DMPG and DPPG in both phases.

Heat capacity curves were obtained for pure lipids and their mixtures, as well as for the same phospholipid mixtures with HIV-1 FP and with HIV-1 FP incubated with E1(64–81), and their phase diagrams were also constructed.

We observed the capacity of HIV-1 FP to modify the properties of the bilayer structure, changing the transition temperature, and the capacity of E1(64–81) to inhibit these modifications. The resulting lipid phase diagram is modified when HIV-1 FP is inserted into the bilayer. However, no difference is observed in the *solidus* curve when HIV-1 FP and E1(64–81) are incubated together. In the *liquidus* curve, small differences could be observed but its shape is more similar to the pure phospholipid curves than to the curve of the phospholipids incubated HIV-1 FP. The higher X_{DPPG}, the more dramatic the effect is.

4. Conclusions

E1(64–81), a synthetic peptide of the E1 structural protein of GBV-C/HGV, shows similar behavior to that observed for other peptide sequences from Hepatitis G structural proteins. E1(64–81) has moderate surface activity that allows it to adopt an α-helix structure at the air–water interface. Its interaction with HIV-1 FP was also studied together with how the presence of E1(64–81) influences the interaction of HIV-1 FP with monolayers and bilayers.

In a dynamic system, HIV-1 FP shows an interaction pattern that is different from that observed for E1(64–81) on phospholipid mono-layers and bilayers. The interaction of both peptide mixtures with the same phospholipid systems demonstrated that the presence of E1 (64–81) reduces or inhibits the action of HIV-1 FP. This is observed in the lipid–peptide miscibility studies as well as in DSC measurements. Moreover, this *in vitro* inhibition of the activity of HIV-1 FP could be explained by the AFM and BAM images which allow us to conclude that the peptide E1(64–81) interacts with HIV-1 FP to form a new structure. These findings could be one more piece of evidence of the inhibition capacity of the E1(64–81) peptide, as observed in other assays (fluorescence spectroscopy), corroborating the hypothesis that synthetic peptides of GBV-C/HGV could inhibit HIV infection. Thus, our results lead us to propose further study of E1(64–81) to explore the correlation between its inhibition capacity *in vitro* and its biological activity *in vivo*. We have therefore started the pertinent studies to establish whether the main trend observed *in vitro* can be related with the biological activity *in vivo*. Furthermore, a more comprehensive analysis of the specific peptide–peptide interaction is in progress.

References

[1] J.N. Simons, T.J. Pilot-Matias, T.P. Leary, G.J. Dawson, S.M. Desai, G.G. Schlauder, A.S. Muerhoff, J.C. Erker, S.L. Buijk, M.L. Chalmers, et al., Identification of two flavivirus-like genomes in the GB hepatitis agent, Proc. Natl. Acad. Sci. U. S. A. 92 (1995) 3401–3405.
[2] J. Linnen, J. Wages Jr., Z.Y. Zhang-Keck, K.E. Fry, K.Z. Krawczynski, H. Alter, E. Koonin, M. Gallagher, M. Alter, S. Hadziyannis, P. Karayiannis, K. Fung, Y. Nakatsuji, J.W. Shih, L. Young, M. Piatak Jr., C. Hoover, J. Fernandez, S. Chen, J.C. Zou, T. Morris, K.C. Hyams, S. Ismay, J.D. Lifson, G. Hess, S.K. Foung, H. Thomas, D. Bradley, H. Margolis, J.P. Kim, Molecular cloning and disease association of hepatitis G virus: a transfusion-transmissible agent, Science (New York, NY) 271 (1996) 505–508.
[3] H.L. Tillmann, M.P. Manns, GB virus-C infection in patients infected with the human immunodeficiency virus, Antiviral Res. 52 (2001) 83–90.
[4] J. Xiang, S. Wunschmann, D.J. Diekema, D. Klinzman, K.D. Patrick, S.L. George, J.T. Stapleton, Effect of coinfection with GB virus C on survival among patients with HIV infection, N. Engl. J. Med. 345 (2001) 707–714.
[5] J. Xiang, S.L. George, S. Wunschmann, Q. Chang, D. Klinzman, J.T. Stapleton, Inhibition of HIV-1 replication by GB virus C infection through increases in RANTES, MIP-1alpha, MIP-1beta, and SDF-1, Lancet 363 (2004) 2040–2046.
[6] C. Voisset, J. Dubuisson, Functional hepatitis C virus envelope glycoproteins, Biol. Cell 96 (2004) 413–420.
[7] M. Sánchez-Martín, J. Amigo, M. Pujol, I. Haro, M. Alsina, M. Busquets, Fluorescence study of the dynamic interaction between E1(145–162) sequence of hepatitis GB virus C and liposomes, Anal. Bioanal. Chem. 394 (2009) 1003–1010.
[8] M.J. Sánchez-Martín, I. Haro, M.A. Alsina, M.A. Busquets, M. Pujol, A Langmuir monolayer study of the interaction of E1(145–162) hepatitis G virus peptide with phospholipid membranes, J. Phys. Chem. B 114 (2010) 448–456.
[9] M.J. Sánchez-Martín, K. Hristova, M. Pujol, M.J. Gómara, I. Haro, M. Asunción Alsina, M. Antònia Busquets, Analysis of HIV-1 fusion peptide inhibition by synthetic peptides from E1 protein of GB virus C, Journal of Colloid and Interface Science 360 (2011) 124–131.
[10] W.C. Chan, P.D. White, Fmoc Solid Phase Peptide Synthesis, Oxford University Press, New Cork, 2000.
[11] E. Kaiser, Rl Colescot, Cd Bossinge, P.I. Cook, Color test for detection of free terminal amino groups in solid-phase synthesis of peptides, Anal. Biochem. 34 (1970) 595.
[12] N. Rojo, M.J. Gomara, M.A. Alsina, I. Haro, Lipophilic derivatization of synthetic peptides belonging to NS3 and E-2 proteins of GB virus-C (hepatitis G virus) and its effect on the interaction with model lipid membranes, J. Pept. Res. 61 (2003) 318–330.
[13] P. Butko, F. Huang, M. Pusztai-Carey, W.K. Surewicz, Membrane permeabilization induced by cytolytic delta-endotoxin CytA from *Bacillus thuringiensis* var. *israelensis*, Biochemistry 35 (1996) 11355–11360.
[14] N.J. Greenfield, Using circular dichroism spectra to estimate protein secondary structure, Nat. Protoc. 1 (2006) 2876–2890.
[15] A. Lobley, L. Whitmore, B.A. Wallace, DICHROWEB: an interactive website for the analysis of protein secondary structure from circular dichroism spectra, Bioinformatics (Oxford, England) 18 (2002) 211–212.
[16] L. Whitmore, B.A. Wallace, DICHROWEB, an online server for protein secondary structure analyses from circular dichroism spectroscopic data, Nucleic Acids Res. 32 (2004) 668–673.
[17] M. Rafalski, J.D. Lear, W.F. DeGrado, Phospholipid interactions of synthetic peptides representing the N-terminus of HIV gp41, Biochemistry 29 (1990) 7917–7922.
[18] E.E. Ambroggio, F. Separovic, J. Bowie, G.D. Fidelio, Surface behaviour and peptide–lipid interactions of the antibiotic peptides, Maculatin and Citropin, Biochim. Biophys. Acta 1664 (2004) 31–37.
[19] R. Maget-Dana, D. Lelièvre, A. Brack, Surface active properties of amphiphilic sequential isopeptides: comparison between α-helical and β-sheet conformations, Biopolymers 49 (1999) 415–423.
[20] J.A. Pérez, J. Cantó, F. Reig, J.J. Pérez, I. Haro, Conformational behavior of the HAV-VP3(110–121) peptidic sequence and synthetic analogs in membrane environments studied by CD and computational methods, Biopolymers 45 (1998) 479–492.
[21] R. Maget-Dana, The monolayer technique: a potent tool for studying the interfacial properties of antimicrobial and membrane-lytic peptides and their interactions with lipid membranes, Biochim. Biophys. Acta (BBA), Biomembr. 1462 (1999) 109–140.

[22] E.E. Conn, P.K. Stumpf, Outlines of Biochemistry, Wiley, New York, 1976.

[23] S.E. Taylor, G. Schwarz, The molecular area characteristics of the HIV-1 gp41-fusion peptide at the air/water interface. Effect of pH, Biochim. Biophys. Acta 1326 (1997) 257–264.

[24] F. Takeda, M. Matsumoto, T. Takenaka, Y. Fujiyoshi, N. Uyeda, Surface pressure dependence of monolayer structure of poly-[epsilon]-benzyloxycarbonyl-lysine, J. Colloid Interface Sci. 91 (1983) 267–271.

[25] M. Kaku, H. Hsiung, D.Y. Sogah, M. Levy, J.M. Rodriguez-Parada, Monolayers and Langmuir–Blodgett films of poly(N-acylethylenimines), Langmuir 8 (1992) 1239–1242.

[26] K. Hac-Wydro, J. Kapusta, A. Jagoda, P. Wydro, P. Dynarowicz-Latka, The influence of phospholipid structure on the interactions with nystatin, a polyene antifungal antibiotic A Langmuir monolayer study, Chem. Phys. Lipids 150 (2007) 125–135.

[27] N. Vila Romeu, J. Miñones Trillo, O. Conde, M. Casas, E. Iribarnegaray, Mixed calcitonin-poly[(D,L-lactic acid)-co-(glycolic acid)] monolayers, Langmuir 13 (1997) 76–79.

[28] C. Larios, J. Miñones, I. Haro, M.A. Alsina, M.A. Busquets, J. Miñones Trillo, Study of adsorption and penetration of E2(279–298) peptide into Langmuir phospholipid monolayers, J. Phys. Chem. B 110 (2006) 23292–23299.

[29] M.A. Alsina, A. Ortiz, D. Polo, F. Comelles, F. Reig, Synthesis and study of molecular interactions between phosphatidyl choline and two laminin derived peptides hydrophobically modified, J. Colloid Interface Sci. 294 (2006) 385–390.

[30] J.T. Davies, E.K. Rideal, Interfacial Phenomena, Academic Press, New York, 1961.

[31] G.L. Gaines, Insoluble Monolayers at Liquid–Gas Interfaces, Wiley-Interscience, New York, 1966, p. 286.

[32] R.E. Pagano, N.L. Gershfeld, A millidyne film balance for measuring intermolecular energies in lipid films, J. Colloid Interface Sci. 41 (1972) 311–317.

[33] P. Bougis, H. Rochat, G. Pieroni, R. Verger, Penetration of phospholipid monolayers by cardiotoxins, Biochemistry 20 (1981) 4915–4920.

[34] D.K. Chattoraj, K.S. Birdi, Absorption and the Gibbs Surface Excess, Plenum Press, New York, 1984 pp. 219,222–223.

[35] M.J. Galvez, M.A. Cabrerizo, A study of the miscibility of bile components in mixed monolayers at the air–liquid interface I. Cholesterol, lecithin, and lithocholic acid, Colloid Polym. Sci. 269 (1) (1991) 77–84.

[36] P. Garidel, C. Johann, A. Blume, The calculation of heat capacity curves and phase diagrams based on regular solution theory, J. Therm. Anal. Calorim. 82 (2005) 447–455.

[37] A.W. Eliasz, D. Chapman, D.F. Ewing, Phospholipid phase transitions. Effects of n-alcohols, n-monocarboxylic acids, phenylalkyl alcohols and quaternary ammonium compounds, Biochim. Biophys. Acta 448 (1976) 220–230.

[38] P. Garidel, C. Johann, A. Blume, Thermodynamics of lipid organization and domain formation in phospholipid bilayers, J. Liposome Res. 10 (2000) 131–158.

[39] S. Mabrey, J.M. Sturtevant, Investigation of phase transitions of lipids and lipid mixtures by sensitivity differential scanning calorimetry, Proc. Natl. Acad. Sci. U. S. A. 73 (1976) 3862–3866.